Proceedings of ASME Turbo Expo 2018: Turbomachinery Technical Conference and Exposition
GT2018
June 11-15, 2018, Oslo, Norway

GT2018-77031

FLOATING SHOCK PLATFORM TESTING OF A MAGNETIC BEARING SUPPORTED CHILLER COMPRESSOR – MEASUREMENTS AND SIMULATION RESULTS

Lawrence Hawkins
Calnetix Technologies
Cerritos, CA, USA

Zhiyang Wang
Calnetix Technologies
Cerritos, CA, USA

Koman Nambiar
Johnson Controls Navy Systems
York, PA, USA

ABSTRACT

Qualification shock testing has been completed for a new chilled water plant developed for the US Navy. The variable speed compressor at the heart of the chiller system includes a direct drive, high-speed permanent magnet (PM) motor, PM bias active magnetic bearings, and a backup bearing system. For MIL-S-901D shock certification, the chiller was mounted on a Navy floating shock platform (barge) and subjected to a standard sequence of four different shock impacts generated from high explosive charges from varying angles and standoff distances. The chiller was fully operational during three blasts and in standby mode for the fourth blast. In the standby mode, the shaft is de levitated and stationary on the backup bearings and the chiller secured. The backup bearing system of the motor absorbed the response to the shock impacts and the magnetic bearings subsequently recovered levitation as designed. The shock testing was simulated using a transient, nonlinear rotordynamic analysis including the magnetic bearing control and saturation features, backup bearings with resilient mounts and associated clearances, and structural dynamic models of the rotor and housing. Compressor/motor housing acceleration measured during the testing was used as the driving input into the simulation. Some rotor position data recorded during shock testing, the simulation approach and comparisons are reported and discussed.

INTRODUCTION

Shipboard cooling loads continue to increase in the U.S. Navy's combatant vessels due to the steadily increasing use of communication and combat electronics. This dictates a need to achieve higher and higher cooling densities in shipboard application of air conditioning plants, with high reliability and maintainability throughout its 40 year service life. Increase in cooling capacity without an increase in the machinery space is required for both new ship construction and in retrofits in existing vessels. Details of the evolution and current direction of naval surface combatant air conditioning plant or chiller technology is discussed by Frank and Martin [1]. Achieving higher cooling densities using centrifugal compressors has resulted in the need to apply high speed sensor less permanent magnet motors with variable speed drives and active magnetic bearings (AMB); implementing these technologies allows elimination of the conventional speed increasing gearing and oil lubricated hydrodynamic bearing systems used in existing refrigerant turbomachinery. The synthesis of these emerging drive & bearing technologies along with a robust compression system & cooling design, with optimized economized thermodynamic cycle and heat transfer has resulted in a chiller design producing unprecedented levels of cooling densities (cooling capacity/installed space) using R134a refrigerant.

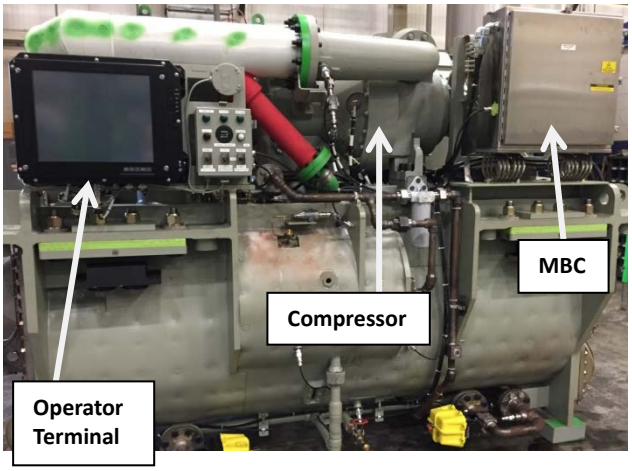

Figure 1: High Efficiency Super Capacity (HES-C) Air Conditioning Plant (Chiller).

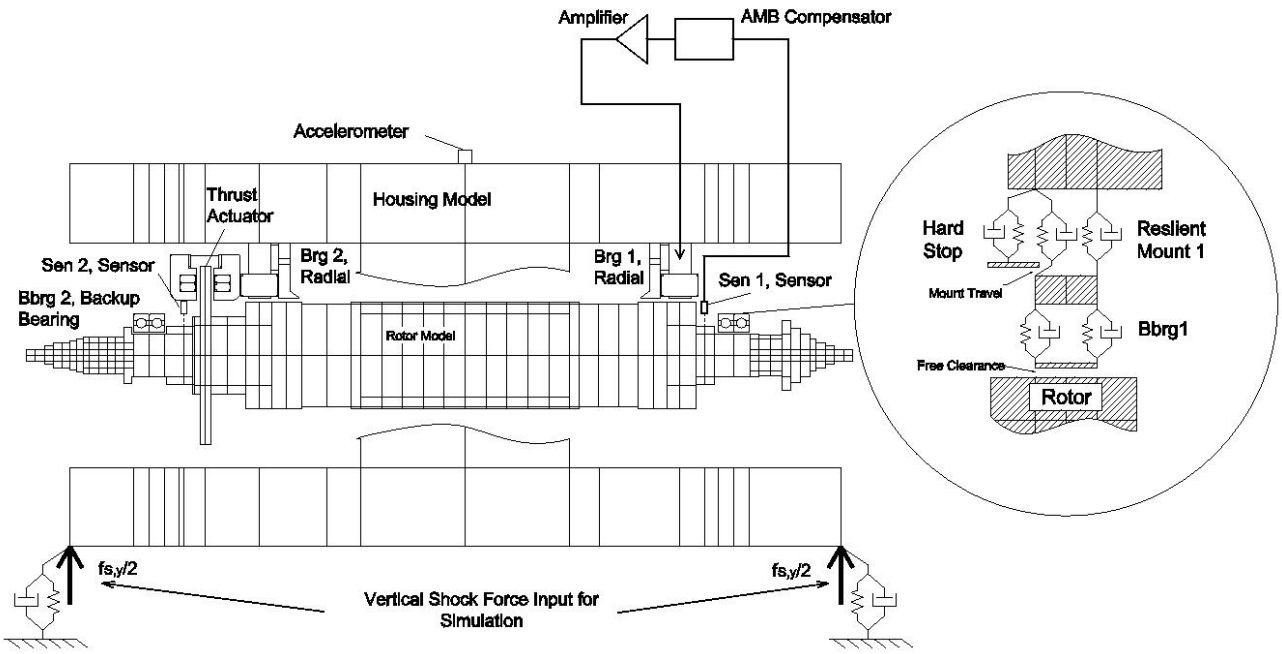

Figure 2. Compressor Model with Rotor, Housing, Magnetic Bearings and Backup bearings

The application of mission critical chillers to naval surface combatants requires the equipment to pass the stringent vibration (MIL-STD-167-1A) and shock (MIL-S-901D) testing [2, 3]. As part of risk mitigation during the development of the new chiller system, the prototype compressor was tested alone, in stand-still (0 rpm shaft speed) and shown to meet the MIL-STD-167 vibration and MIL-S-901D shock requirements. The vibration testing for this phase, along with other system information, was reported by Hawkins [4]. Subsequently, the Production Prototype High Efficiency Super Capacity (HES-C) Chiller, Fig. 1, was developed and satisfactorily completed the MIL-STD-167-1 Vibration Testing and the MIL-S-901D Shock Testing (Grade A, Class II). These tests were performed with the complete chiller system in normal operation.

The size and weight of the new chiller necessitates shock testing be performed using the Heavy Weight or Floating Shock Platform (FSP). For this test the HESC Chiller was installed on a FSP and subjected to a series of four shock impacts from high-explosive charges positioned 24-feet under the water. As dictated by the standard, one blast was 40-feet from the front of the floating platform and the other three blasts were 30-feet, 25-feet and 20-feet respectively from the side of the platform. The chiller was operating during three blasts and in standby mode for one blast. The backup bearing system of the compressor absorbed the shock impacts; the magnetic bearings recovered levitation as designed; and the motor performed without any issue. For MIL-STD-167-1A vibration testing, the chiller was mounted on a shaker platform and driven at varying frequencies and amplitudes in three axes while operating.

Data collected during the shock testing is presented here including Magnetic Bearing Controller (MBC) measured rotor/housing relative displacements, commanded currents, and coil currents as well as customer provided housing acceleration. Additionally, development of a realistic simulation model which predicts the behavior of the active magnetic bearings under shock loading has been undertaken and is presented in this paper. This effort is intended to improve understanding of the rotor/housing, active magnetic bearings, and back up bearing system during a shock event. As a result, the existing FSP Shock Test results can be extended to evaluate changes to magnetic bearing and back up bearing design and application for future platforms. This will serve as valuable risk mitigation and in some cases help eliminate FSP shock testing for similar applications.

COMPRESSOR DESIGN

In the HES-C chiller system, the compressor is mounted on top of the chiller heat exchanger (Fig. 1). The MBC is mounted to the skid using standard wire rope shock isolators. The system control devices and operator interfaces are mounted to the same skid. The rotordynamic model of compressor rotor and housing is shown in Fig. 2. The two-stage compressor has a stage on either end of the machine (double overhung). The high-speed permanent magnet motor is centrally located and is supported by two identical radial permanent magnet (PM) bias magnetic bearings, Fig. 3. There is an electromagnetic thrust bearing on one end of the machine. Selected characteristics of the magnetic bearings are summarized in Table 1. The non-thrust end radial bearing is designated Brg 1, with axes x1 and y1, the thrust end radial bearing is designated Brg 2, with axes x2 and

y2, and the thrust bearing is designated Axial with axis is z. The magnetic bearing system is designed to accommodate the rotor weight, aerodynamic thrust loads, transient unbalance loads, ship motion and inclination, and environmental vibration loads. Hawkins [4] described the sizing to meet vibration loads per MIL-STD-167 as well as risk mitigation testing of the stand – alone compressor. The complete and operating chiller/compressor system (chilled water A/C plant), underwent MIL-STD-167 vibration testing in January, 2017, prior the shock testing described below.

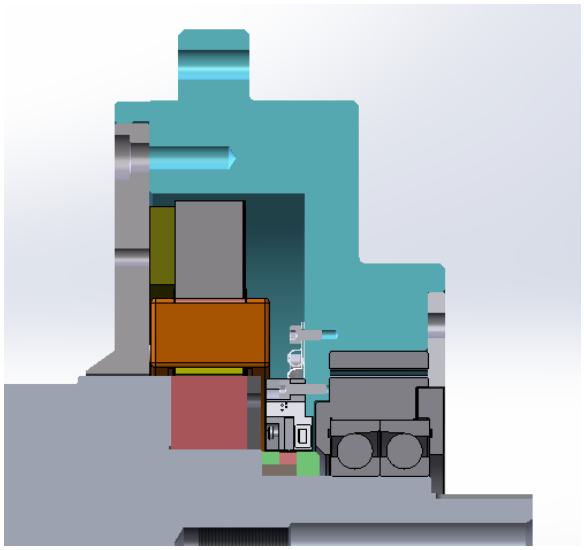

Figure 3. Arrangement of radial AMB Brg1 and backup bearing Bbrg1 (non-thrust end).

TABLE 1 MAGNETIC BEARING SYSTEM CHARACTERISTICS

Bearing	Radial Bearings		Thrust Bearing
Bearing Ref. Name	Brg 1	Brg 2	Axial
Coordinate Names	x1,y1	x2,y2	z
Load Capacity, N (lbf)	3,122 (700)		6,244 (1,400)
Force Constant, N/A (lbf/A)	365 (82)		801 (180)
Negative Stiffness, N/mm (lbf/in)	6,150 (35,000)		7,125 (40,000)
Magnetic Bearing Air Gap, mm (in)	>0.63 (>0.025)		>0.63 (>0.025)

All industrial AMB supported machines include a backup bearing system to support the rotor during non-operation of the AMB and in the event of a process or environmental overload of the AMB. In this machine, the backup bearing system provides the primary reaction against shock loads. The shock design requirement was specified by the chiller manufacturer in terms of peak housing acceleration. This specification was based on actual FSP (barge) instrumented test data from legacy equipment. The levels far exceed the shock levels experienced by commercial and industrial equipment. This requirement was the key driver for the sizing of the backup bearings. The backup bearing system consists of resiliently mounted, duplex pairs of angular-contact ball bearings mounted on each end of the machine. The radial backup bearing, Bbrg 1, is shown in Fig. 3. The configuration is typical for an AMB application: steel races, a full complement of ceramic balls, and grease film lubrication.

For the simulation model discussed below, the backup bearing system is modelled as shown in the inset to Fig. 2. There is a free clearance between the inner rings of the bearings and the rotor landing surfaces such that they are not normally in contact. The resilient mount comprises an arrangement of metal springs configured to provide a monotonically increasing radial stiffness from initial contact until the hard stop is reached. Another feature of the mount provides Coulomb friction damping. Radial clearances and relative stiffness values for the backup bearings and resilient mount are given in Table 2. The axial free clearance is ±0.178 mm (±0.007 in). As a rule of thumb, the authors generally set initial resilient mount stiffness such that static deflection from rotor weight and negative stiffness is 0.025-0.051 mm (0.001-0.002 in). The stiffness values are shown relative to *Kb*, the radial stiffness (inner ring to outer ring) of the duplex pairs, as we are required to keep the actual stiffness values used in this program confidential. Contact forces were calculated using a linear visco-elastic impact model which treats the impact as half of a linear damped vibration cycle [Bartha, 5].

TABLE 2 RADIAL BACKUP BEARING AND MOUNT CHARACTERISTICS

Radial Clearances and Spring Travel	
Free Clearance, mm (in)	0.152 (0.006)
Radial Bearing Deflection at Peak Load, mm (in)	0.076 (0.003)
Resilient Mount Travel, mm (in)	0.178 (0.007)
Relative Radial Stiffness Values	
Radial Bearing Stiffness (duplex pair),	Kb
Radial Resilient Mount Stiffness	0.15Kb → 0.50Kb
Radial Hard Stop Stiffness	5.0Kb

The magnetic bearing position control includes a basic PID regulator and additional bi-quad filters to shape the frequency response for suitable control robustness. As the system design dictates that the backup bearings carry the main shock load, the magnetic bearing control is optimized for stability during normal operation. The MBC is also responsible for overload detection and recovery from shock. The MBC continuously monitors rotor/housing relative displacement and for this system triggers a fault and rotor delevitation if excess displacement is detected for over 0.25 seconds. After a customer defined delay, *t_delay* seconds, the fault is cleared, resulting in a relevitation attempt. If relevitation is successful, operation can continue as programmed. A similar approach was described by Khatri [6] for a different system subject to impulse overloads.

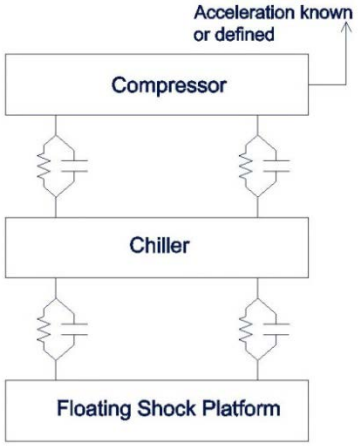

Figure 4. System model for the shock test.

SHOCK TESTING

System Model

A commonly used structural model to represent the heavyweight shock test [7] is shown in Fig. 4 in a slightly modified form. The chiller system is mounted via isolation mounts on a barge (the Floating Shock Platform, FSP) which is floated in a large body of water for the test. The compressor housing is mounted on the chiller via a compliance that is not well known. However, the acceleration of the relatively rigid compressor housing is known as it was measured during the test. Also, for future use of the simulation tool for follow-on design purposes, the compressor housing acceleration will be defined. In either case, the simulation can use the rotordynamic system model of the compressor shown in Fig. 2 in isolation. The housing acceleration, as measured or defined, is the driving input into the analysis.

Test Conditions

In the MIL-S-901D shock test, the HES-C chiller was mounted on the FSP and subjected to a standard sequence of four different shock impacts generated from high explosive charges. Each test in the sequence is referred to by a Shot number as identified in Table 3 below. For Shots 1, 2, and 4 the chiller system was operated at a capacity dictated by reservoir water temperature. The "warm" water input to the chiller during testing was drawn from the reservoir, then cooled by the chiller and discharged back into the reservoir. The compressor was operated at less than maximum operating speed due to the relatively cool waters of the reservoir in January. The compressor design is capable of operating at much higher speeds at maximum thermal load conditions. In each of four tests, a 60 pound charge of High Blast Explosive was detonated at 24 foot depth each with a different (horizontal distance from blast center to near edge of barge) per Table 3.

The testing order was Shot 2,3,4,1 per the Navy's testing protocol. After each test, the system was shut down and the chiller system was inspected for refrigerant leaks or other damage. Meanwhile, backup bearing clearance checks and magnetic bearing transfer function measurements were performed to verify integrity of these systems. Additionally, data collected by the MBC during the test – the fault/event log and high frequency measurements (5 kHz) of sensor position, coil current and commanded current – were reviewed. Following the inspections and data review, the system was returned to operation each time and normal operation was verified. No observable change in backup bearing clearance, backup bearing rolling orbits, or rotor unbalance response were found after any of the four tests.

TABLE 3 TEST SEQUENCE

Shot	Standoff, ft (m) (horizontal distance from barge)	Shot direction	Chiller Compressor Operating Condition
1	40 (12.2)	Fore-aft	Normal Operation
2	30 (9.1)	Athwartship	Normal Operation
3	25 (7.6)	Athwartship	Standby (de-levitated)
4	20 (6.1)	Athwartship	Normal Operation

Test Results

The Fore/Aft test, Shot 1, was the least severe of the four tests due both to the large standoff and orientation of the shock along the main barge axis. Although hard backup bearing contact was made following this shock event, the rotor remained levitated throughout this event and no fault was triggered. During Shot 3, the magnetic bearings & motor were de-energized with the stationary rotor supported on the backup bearings per the Navy's test protocol. No data was recorded during this test but post shock measurements did not identify any problems with the magnetic bearings and its backup bearing system. The most severe test was Shot 4 as this was the closest blast (smallest standoff) and the orientation was lateral to the main barge axis. The review of test and simulation results below focus on Shot 4. Behavior of the rotor and magnetic bearing system during Shot 2 was similar to Shot 4 except that maximum relative rotor/housing displacement recorded at the position sensors was smaller compared to the Shot 4.

Measurements from the shot 4 test are shown in Figs. 5-11. Available data includes compressor housing acceleration, relative rotor/housing displacement from the position sensors, commanded current and coil current. Figure 5 show the vertical, horizontal, and vector magnitude acceleration non-dimensionalized to the peak measured acceleration. This data is from a tri-axial sensor mounted at the top of the housing at roughly the axial center of the rotor (see Fig. 2). The vertical acceleration is higher than horizontal due to the short horizontal standoff of this shot. The vertical acceleration can be described as an initial pulse, with each successive half pulse smaller and longer in duration. The peak housing acceleration vector relative to global axes (X,Y) and the magnetic bearing axes (x1, y1 shown) in the inset to Fig. 5.

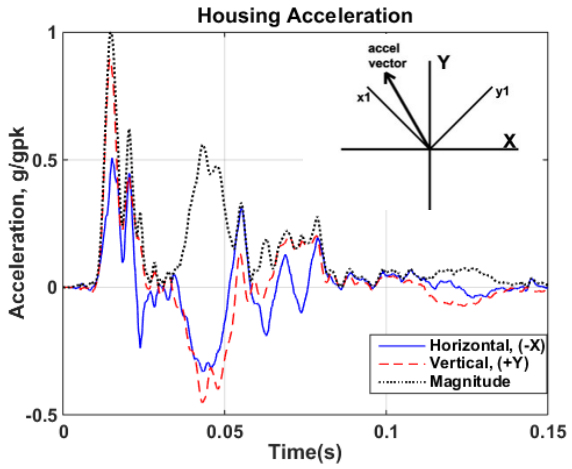

Figure 5. Measured housing acceleration, g/g_pk.

Figures 6-9 show a series of 4 orbit plots of relative rotor/housing displacement, all from the Brg1 position sensors. On each plot, the earliest point in time is marked by a *dot* and the last point in time is marked by an *x*. Figure 6 shows the first 0.090 sec of motion following the shock which includes the three significant half pulses from the acceleration measurement. There are two dashed circles shown on this plot representing: 1) the free backup bearing clearance of 152.4 µm (0.006 in), and 2) the maximum radial rotor housing travel (at the backup bearings) before engaging the hard stop 406.4 µm (0.016 in). The maximum travel includes the free clearance, full deflection of the resilient mount before hard stop, and relative backup bearing inner/outer ring deflection at the load associated with full mount deflection. In Fig. 6, there are several excursions beyond this hard stop threshold; however, note that the measured position data is from the position sensor axial location, and doesn't include additional possible deflection of the rotor between the sensor and backup bearing.

Note that the initial motion detected is between negative x1 and y1 axes, but closer to x1. This is consistent with the housing acceleration vector shown in Fig. 5 since the housing is being accelerated along the positive direction toward the rotor which is viewed by the sensors as the rotor moving in the negative directions toward the housing.

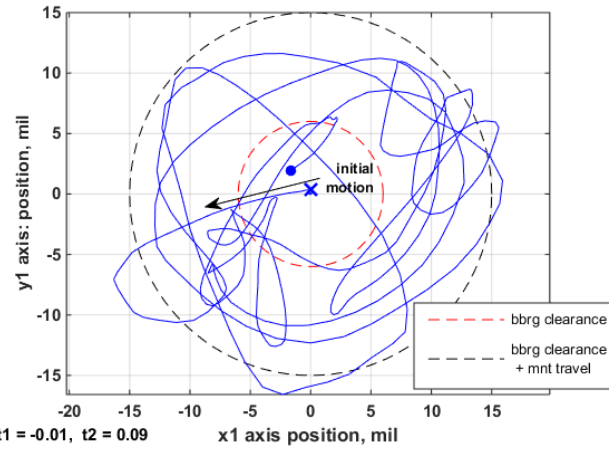

Figure 6. Shot 4 – Shock impact with initial relative rotor/hsg motion measured from Brg 1 position sensors.

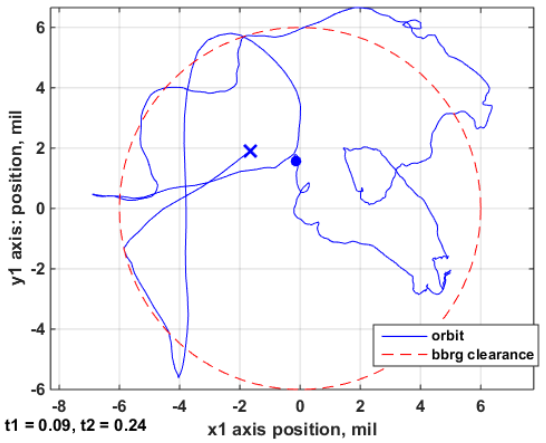

Figure 7. Shot 4 – Rotor bouncing and partial recovery measured from Brg 1 position sensors.

Figure 7 shows data from 0.090 sec to 0.240 sec after initiation of the shock. The rotor motion has attenuated substantially, but is still in and out of contact with the backup bearings. The MBC position fault detection scheme has a delay timer that triggers when the rotor position exceeds the fault limit (127 µm/0.005 inch in this case) and trips if the rotor position exceeds the fault limit during a specific portion of the delay period. In this case, the fault trips and de-levitates the rotor 0.250 sec after the delay timer triggers (Fig. 8). After delevitation, the rotor executes several forward whirl orbits, and settles to a low frequency rocking motion nearly vertically down in the backup bearings. After the customer defined reset period, with rotor speed greater than 5,000 rpm, the rotor is relevitated in a stable manner as shown in Fig. 9. Following relevitation, the compressor operation continues as designed.

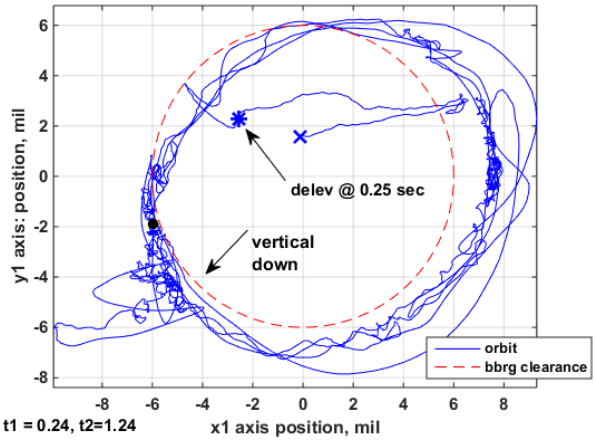

Figure 8. Shot 4 - Drop fault trips 0.250 sec after initial impact and rotor is de-levitated. Measured from Brg 1 position sensors.

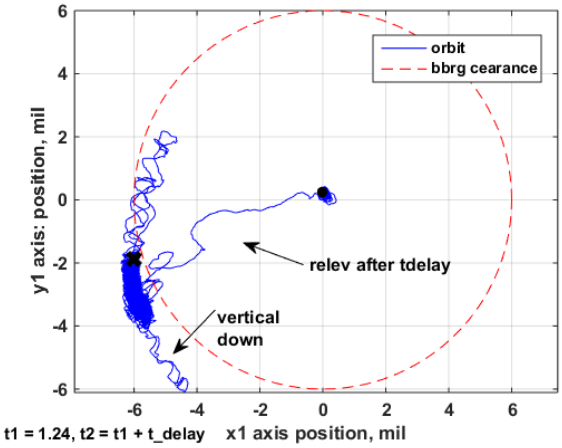

Figure 9. Shot 4 - AutoReset clears fault after t_delay seconds to relevitate rotor. Measured from Brg 1 position sensors.

It is also instructive to view the data versus time. Figs. 10 and 11 show time history data from the x1 position sensor. Position, current and commanded current are shown on both plots and the time axis has been shifted to put the initial rotor reaction to shock at t=0 sec. Immediately after the shock impact the bearing hits current limit and the amplifier saturates for a few cycles; this is evidenced by the constant current vs. time slope of the coil current which of course causes the coil current to lag the command. The primary response frequency of the rotor is 175 Hz, which approximately coincides with the expected rigid body natural frequency of the rotor mass on the average mount stiffness (the stiffness increases with displacement amplitude). This frequency is estimated by measuring the time for the first three cycles. Within about 0.060 to 0.070 sec – about the duration of the first three major half pulses of the housing shock response – the amplifier is out of saturation and the bearing is no longer in current limit. At this point, the control is beginning to stabilize the rotor, but the motion is still large enough such that the position fault triggers

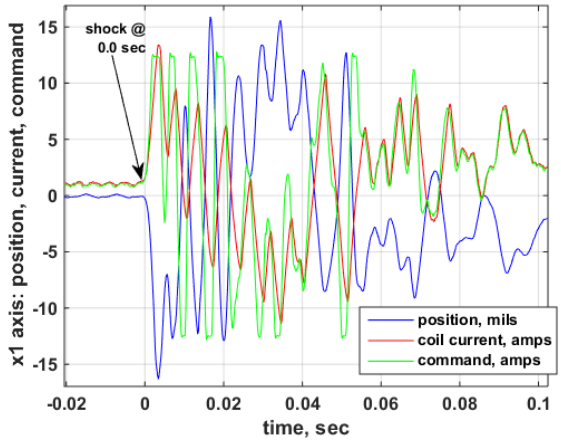

Figure 10. Measured magnetic bearing reaction to Shot 4, x1 axis: sensed position, commanded current and coil current.

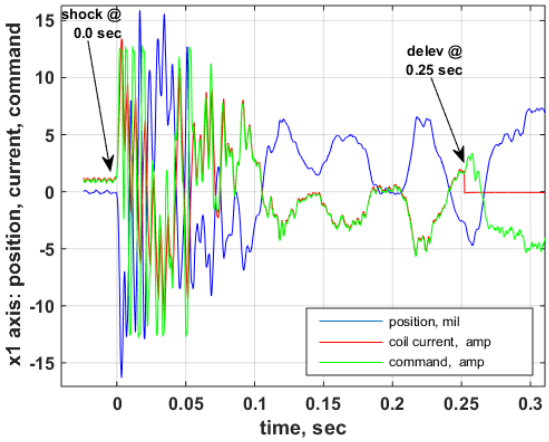

Figure 11. Measured magnetic bearing reaction to Shot 4, x1 axis: sensed position, commanded current and coil current.

at 0.25 seconds and the rotor is de-levitated by the MBC. For this particular case, a longer fault delay may have allowed the MBC to recover levitation without the delevitation and reset.

Following the completion of the four shock tests, key elements of the chiller system and compressor were inspected for potential damage. Of primary interest was the condition of the backup bearings. The backup bearings and resilient mount cartridge were removed from the machine and visually inspected. Some of the observations were:

1) The bearings bores, thrust end bearing inner ring axial faces, radial and axial shaft landing surfaces all had normal very light scoring of the contact surfaces.
2) No evidence of Brinelling or other significant raceway defects were identified by visual inspections or rolling the assembled bearings by hand.
3) The grease lubrication was in place and in good condition and showed no significant discoloration.

Based on the visual inspection and the relatively benign test results, it was determined that further disassembly was not warranted. The backup bearings were re-installed in machine and subsequently post shock endurance testing of the chiller was completed without consequence. The Navy and chiller manufacturer both observed that all evidence was that the shock test caused no loss of the designed equipment service life. This is in contrast to the experience of the chiller manufacturer after shock testing similarly mounted traditional compressors on oil film bearings. The oil film bearing machines take the impact of the shock impulse on the *operational bearings*. Typically mechanical distress will be seen on the both the journals and the hydrodynamic bearing surfaces due to metal-to-metal contact. This wear results in some reduction of service life of the bearings following a shock test or shock event.

SHOCK SIMULATION

A transient, non-linear simulation tool was used to predict the performance of the complete compressor system to the shock input. The overall goal of this simulation effort is to show that the rotor displacements, AMB control behavior, and backup bearing system performance can be adequately predicted using a known housing acceleration profile as the driving input. This would allow the simulation tool to be used in the future for risk mitigation analysis and evaluation of design modifications.

Simulation Model

The rotordynamic equations of motion for the compressor, which is in general a coupled, flexible rotor/housing system, is:

$$\begin{bmatrix} \mathbf{M}_R & 0 \\ 0 & \mathbf{M}_C \end{bmatrix} \begin{Bmatrix} \ddot{\mathbf{q}}_R \\ \ddot{\mathbf{q}}_C \end{Bmatrix} + \begin{bmatrix} \mathbf{D}_R + \mathbf{G}_R & 0 \\ 0 & \mathbf{D}_C \end{bmatrix} \begin{Bmatrix} \dot{\mathbf{q}}_R \\ \dot{\mathbf{q}}_C \end{Bmatrix} + \begin{bmatrix} \mathbf{K}_R + \mathbf{K}_{B1} & \mathbf{K}_{B2} \\ \mathbf{K}_{B3} & \mathbf{K}_C + \mathbf{K}_{B4} \end{bmatrix} \begin{Bmatrix} \mathbf{q}_R \\ \mathbf{q}_C \end{Bmatrix} = \begin{Bmatrix} \mathbf{f}_{mb,R} \\ \mathbf{f}_{mb,C} \end{Bmatrix} + \begin{Bmatrix} \mathbf{f}_{ext,R} \\ \mathbf{f}_{ext,C} \end{Bmatrix} \quad (1)$$

where the subscripts *R* and *C* refer to rotor and housing (casing) structures, **M**, **D** and **K** are the mass, damping and stiffness matrices, respectively, for the separate rotor and housing structures, $\mathbf{G_R}$ is the rotor gyroscopic matrix containing skew symmetric products of polar inertia and spin speed, $\mathbf{K_{Bi}}$, is a sparse matrix containing entries for linear connecting elements such as the passive actuator negative stiffness or conventional bearings, and **q** is the physical displacement vector. Magnetic bearing control forces are applied through the force vector, $\mathbf{f}_{mb}$. The external force vector $\mathbf{f}_{ext}$ can include linear, nonlinear and/or time dependent forces such as rotor unbalance forces, static loads, external shock loads, or loads from nonlinear interconnecting elements such as backup bearings.

For conciseness, Eq. 1 is rewritten as follows

$$\mathbf{M}\ddot{\mathbf{q}} + \mathbf{D}\dot{\mathbf{q}} + \mathbf{K}\mathbf{q} = \mathbf{f}_{mb} + \mathbf{f}_{ext} \quad (2)$$

where for example

$$\mathbf{M} = \begin{bmatrix} \mathbf{M}_R & 0 \\ 0 & \mathbf{M}_C \end{bmatrix}, \ \mathbf{D} = \begin{bmatrix} \mathbf{D}_R + \mathbf{G}_R & 0 \\ 0 & \mathbf{D}_C \end{bmatrix}.$$

Similar substitutions apply for the stiffness matrix, the vibration vectors and the force vectors. Eq. 2 can be rewritten as follows:

$$\ddot{\mathbf{q}} = -\mathbf{M}^{-1}\mathbf{D}\dot{\mathbf{q}} - \mathbf{M}^{-1}\mathbf{K}\mathbf{q} + \mathbf{M}^{-1}\mathbf{f}_{mb} + \mathbf{M}^{-1}\mathbf{f}_{ext} \quad (3)$$

In the simulation tool, Eq. 3 is numerically integrated using the Newmark-Beta method [Bathe, 8]. The transient and/or nonlinear forces are updated at each integration step and added to the force vector. The linear forces are updated at each integration step – or at a lower rate if so defined – and added to the force vector. Modelling backup bearing clearance, amplitude dependent stiffness, a short term shock input, or magnetic bearing saturation characteristics are straightforward with this approach. For example, if after a given time step, the relative displacement between the rotor and backup bearing inner ring is less than the free clearance, there is no force applied at the backup bearing location for that time step. If the relative displacement exceeds the free clearance, then the force applied at the backup bearing location will depend on the radial displacement beyond the free clearance and the non-linear force deflection characteristic defined for the backup bearing. The integration time step for the structural dynamic elements was varied from 1 to 10 μsec for evaluation and subsequently 10 μsec was used for the analysis results reported here.

The magnetic bearing compensator is realized using the same discrete, z domain transfer function coefficients that are used in the MBC digital controller. The magnetic bearing position and current control loops in the simulation are updated at 80 μsec and 40 μsec intervals respectively – just as in the actual MBC hardware. At each integration time step for the structural dynamic model, the most recent values from each current control loop is multiplied by the appropriate actuator gain (to get force) and added to $\mathbf{f}_{mb}$.

Each time the current is updated, the momentary current slew rate, *di/dt*, is compared to the maximum slew rate calculated per Vischer [9]:

$$di/dt)_{max} = (V_{bus} - R\,i - K_i v)/L \quad (4)$$

where V_{bus} is the overhead voltage, *R* is coil resistance, *i* is coil current, K_i is force/current factor, *v* is max whirl velocity, and *L* is coil inductance. The momentary current slew rate exceeds the maximum defined by Eq. 4 it is clamped to the maximum.

The system model, shown in Fig. 2, includes these elements:

1) Rotor: a linear, structural dynamic model created per standard industry practice,
2) Housing: a distributed but rigid housing structural dynamic model,
3) Compensator: a z-domain magnetic bearing compensator with integrator saturation and current limit features that match the real system,
4) Actuator: a simple actuator/amplifier model that includes amplifier saturation (slew rate limit),
5) Backup bearings: includes rotor-to-inner ring free clearance, damping, non-linear force/deflection curve, and
6) Resilient mount: includes damping, non-linear force/deflection curve, and hard stop stiffness.

To facilitate the analysis, the compressor connections to ground in Fig. 2 were made relatively soft such that the

compressor housing rigid body natural frequencies were much lower than the primary shock motion (around 20 Hz). This allowed the simulation driving forces in the vertical and horizontal directions, f_{Sx} and f_{Sy}, to be calculated from:

$$f_{S,x} = m_{cas}\,\ddot{x}_{cas} \qquad (5)$$
$$f_{S,y} = m_{cas}\,\ddot{y}_{cas}$$

where m_{cas} is the mass of the housing in the simulation model, and $\ddot{x}_{cas}$ and $\ddot{y}_{cas}$ are the *measured* housing accelerations versus time in the horizontal and vertical directions (shown in Fig. 5). In the physical system, the housing connection to the chiller is certainly much stiffer than modelled here; however, by calculating the driving forces in this way, the housing motion is directly prescribed, allowing the compressor model to be analyzed in isolation. Figure 12 shows a comparison of the measured vertical acceleration, $\ddot{y}_{cas}$, to the acceleration predicted by the simulation model using f_{Sx} and f_{Sy} as force inputs. The correlation is quite good with a peak value 2.5% less than the measured value. The match for the measured and predicted horizontal acceleration is similar. This result is quite adequate for the purposes of the analysis.

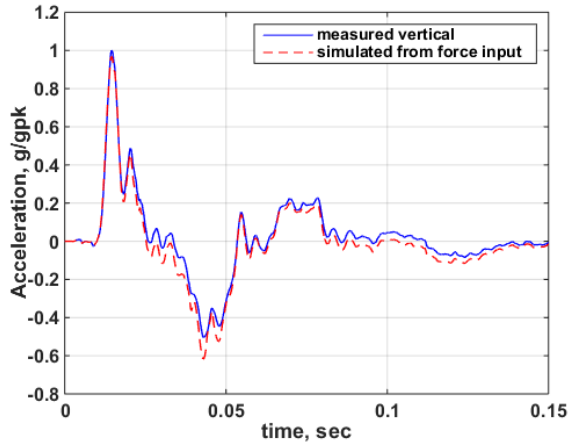

Figure 12. Comparison between measured and simulated housing acceleration in vertical axis.

Simulation Results

Figures 13-18 show results from the Shot 4 shock simulation. Figures 13-15 show displacement orbit plots of the shock impulse and the following 1.24 seconds. On each plot, the earliest point in time is marked by a *dot* and the last point in time is marked by an *x*. The predicted rotor trajectory due to the shock impact (Fig. 13) is similar to the test data (Fig. 6). The peak predicted excursion is 0.0187, about 5.5% higher than the measured peak of 0.0177 in. The predicted peak response is also sharper than the measured peak response. Several factors may contribute to these differences: 1) the piecewise linear force/deflection curve used for the resilient mount is relatively simple (based on three FEA analysis points, 2) the resilient mount model is axisymmetric whereas the physical hardware is only approximately symmetric, 3) the housing model is rigid whereas the real housing although stiff has some flexibility, and 4) measured housing acceleration is only available for one location on the housing. During the period when the magnetic bearing is attempting to recover levitation, Fig. 14, the rotor is bouncing in and out of the free

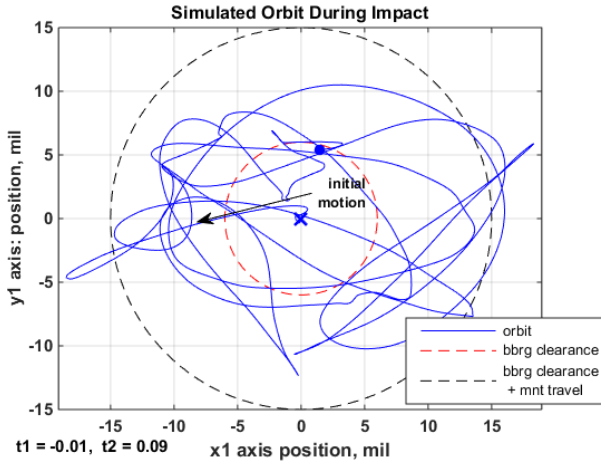

Figure 13. Shot 4 – Predicted Bbrg 1 shock impact with initial relative rotor/hsg motion shown.

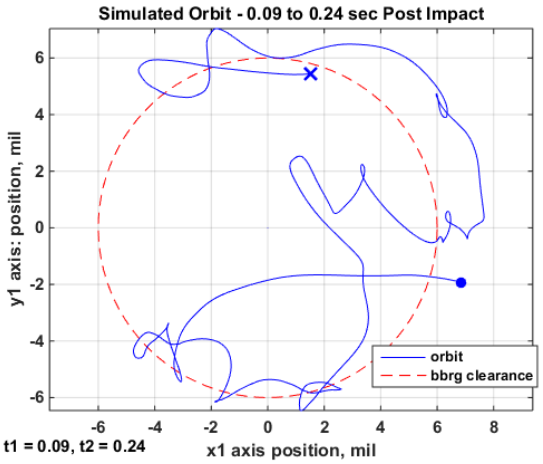

Figure 14. Shot 4 - Predicted Bbrg 1 bouncing to secondary shocks and partial recovery.

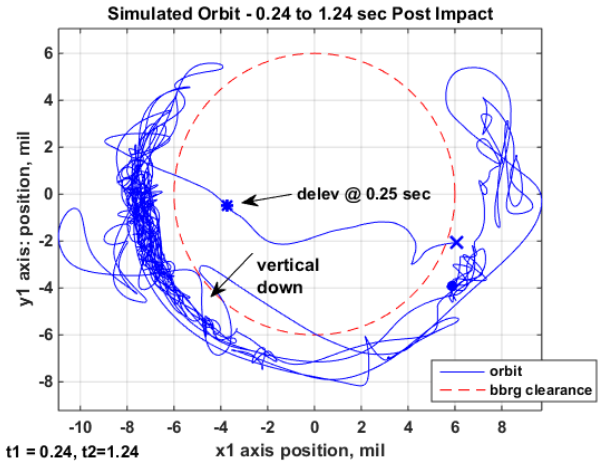

Figure 15. Shot 4 - Predicted Bbrg 1 delevitation and rocking on backup bearing.

clearance space, similar to the measurement of Fig. 7. After delevitation (Fig. 15), the simulation predicts the rotor dropping to the backup bearings, executing a few partial whirl orbits and settling to a rocking motion at the bottom of the bearing. This is similar to the measured response in Fig. 8.

Figure 16 shows predicted time history for axis x1 for comparison to the measured data in 10. The amplifier saturation and max current rate correlate well as they should since the hardware characteristics are well defined and easy to model. Also, the response frequency of the first four cycles is 160 Hz, about 10% lower than the measured value (175 Hz). This indicates the effective stiffness of the actual resilient mount over a cycle may be about 20% stiffer than expected.

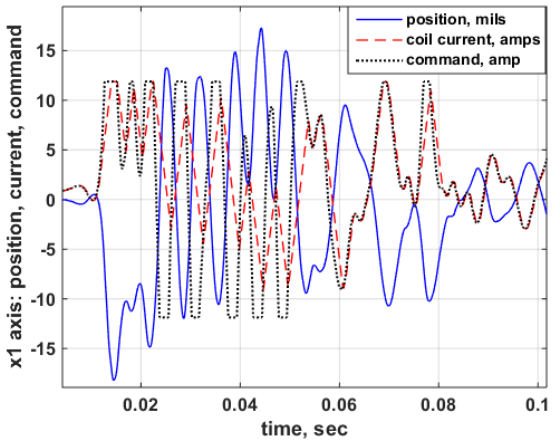

Figure 16. Shot 4 - Predicted magnetic bearing response, x1 axis: position, commanded current and coil current.

Figure 17 shows predicted bearing loads for the radial end bearing pair and for the combo end bearing pair. The results are non-dimensionalized by dividing by the load *F**

$$F^* = \ddot{x}_{cas,pk}\, m_{rot}/2 \qquad (6)$$

where $m_{rot}/2$ is half the rotor mass, and $\ddot{x}_{cas,pk}$ is the peak housing acceleration. The housing acceleration is used because it is generally a design specification or a measured value (as in this paper). The load *F** is the max load that each bearing pair would see if the rotor is accelerated at the peak housing acceleration; so the results indicate that the peak rotor acceleration is greater than the peak housing acceleration. This is expected since the housing, together with the backup bearings, impact the stationary rotor with an initial velocity that must be also picked up by the rotor. Figure 18 shows the rotor and housing velocities overlaid on the Bbrg1 bearing load. The velocities are non-dimensionalized by the peak rotor velocity, V*. The plot clearly shows that the peak bearing loads occur when the rotor and housing velocities are equal, and the rotor velocity is increasing relative to the housing velocity.

The comparison of the predicted results to measurements indicates that the simulation tool can provide a reasonable prediction of magnetic bearing and backup bearing performance during a shock event. Thus the tool can be used for evaluating changes to the system or for evaluating a new design. Of particular interest in the future is examining the influence of resilient mount stiffness and damping, characteristics of resilient mount amplitude dependence (softening, stiffening), backup bearing free clearance, and magnetic bearing control strategies.

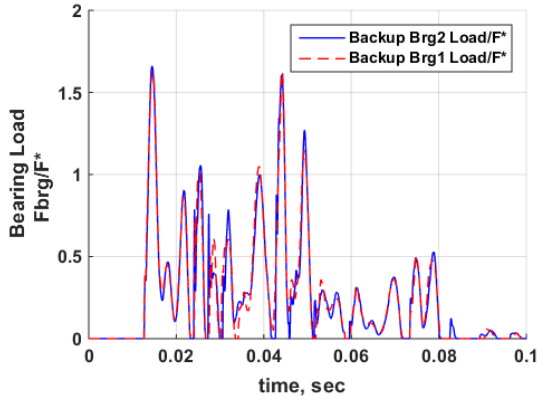

Figure 17. Shot4 - Predicted backup bearing loads, non-dimensionalized.

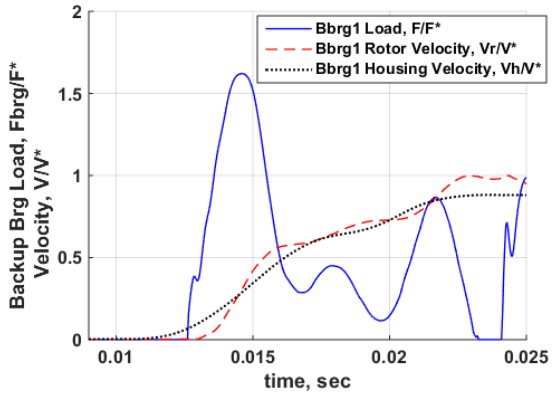

Figure 18. Shot 4 - Predicted backup bearing 1 loads vs. rotor and housing velocity.

CONCLUSIONS

Qualification shock testing per MIL-S-901D has been completed on the new HES-C chiller for the US Navy. A key part of the chiller is an integrated high speed two stage centrifugal compressor supported on active magnetic bearings along with a backup bearing system designed to absorb shock overloads. Both bearing systems performed as designed with the magnetic bearings delevitating the rotor as expected to the sustained dynamics of the two strongest levitated shocks. The backup bearing system compressed and absorbed the shock

overloads as intended, limiting forces to acceptable levels, thereby preventing damage to any rotating or stationary components. Post-test inspections showed that the backup bearings which experienced limited contact time had no raceway Brinelling or other signs of distress. The axial contact surfaces also were in good condition. No changes in backup bearing clearances, rotor balance levels, or in magnetic bearing system frequency response measurements were observed in the post test evaluations.

The Navy and chiller manufacturer both observed that all evidence was that the shock test caused no loss of the designed equipment service life. This is in contrast to the experience of the chiller manufacturer after shock testing similarly mounted traditional compressors on oil film bearings.

A simulation model was developed to predict response of the rotor, magnetic bearing system, and backup bearings to the worst case shock event. Measured housing acceleration from Shot 4 of the FSP shock test, was used as a driving input into the analysis. The predicted rotor displacements and magnetic bearing control responses correlated well with the measured values. The predicted peak displacement response was about 8% higher than measured, a result that is on the conservative side and certainly adequate for design purposes. These results indicate that the simulation tool can provide a good prediction of magnetic bearing and backup bearing performance during a shock event. The tool will be used in the future for evaluating changes to the system or for evaluating new designs.

ACKNOWLEDGMENTS

The work reported here supported U.S Navy Contract N65540-14-D-0006, Program Manager: Neil Antin; Naval Sea Systems Command, Washington, DC. The United States Government retains, and by accepting the article for publication, the publisher acknowledges that the United States Government retains, a non-exclusive, paid-up, irrevocable, worldwide license to publish or reproduce the published form of this work, or allow others to do so, for United States Government purposes.

REFERENCES

[1] Frank M. and Martin K., 2016, “Chilled Water Challenges, the Evolution of Systems used on Naval Surface Combatants”, *Marine Technology*, January, ASNE.

[2] Naval Sea Systems Command, 2005, MIL-STD-167-1A, *Military Standard, Mechanical Vibrations of Shipboard Equipment*, November

[3] Naval Sea Systems Command, 1989, MIL-S-901D, *Military Specification, Shock Tests, H.I. (High Impact) Shipboard Machinery, Equipment and Systems, Requirements For*, March.

[4] Hawkins, L., Khatri, R., Nambiar, K., 2015, “Test Results and Analytical Predictions for MIL-STD-167 Vibration Testing of a Direct Drive Compressor Supported on Magnetic Bearings”, *J. of Engineering for Gas Turbines and Power*, GTP-14-1441, Vol 137, No. 5, May.

[5] Bartha, A. R., 2000, “Dry Friction Backward Whirl of Rotors,” Dissertation ETH No. 13817, ETH Zurich.

[6] Khatri, R., Hawkins, L., Bazergui, C., 2015, “Demonstrated operability and reliability improvements for a prototype high- speed rotary-disc atomizer supported on active magnetic bearings”, *ASME Turbo Expo 2015*, Paper GT2015-43803, June, Montréal, Canada.

[7] Del Rosario, J. and Murphy, S., 2003, “Environmental Engineering Grade A Shock Tests”, *Oceans 2003 MTS/IEEE Conference*, September, San Diego, CA, USA.

[8] Bathe, K.J., 1996, *Finite Element Procedures in Engineering Analysis*, Prentice-Hall, New Jersey.

[9] Vischer, D., Bleuler, H., 1990, “A new approach to sensorless and voltage controlled AMBs based on network theory concepts”, *Proceedings 2nd International Symposium on Magnetic Bearings*.

